Perica Paunović[1]
Faculty of Technology and Metallurgy,
SS Cyril and Methodius University,
Rudjer Bošković Street, 16,
Skopje 1000, R. N. Macedonia
e-mail: pericap@tmf.ukim.edu.mk

Anita Grozdanov
Faculty of Technology and Metallurgy,
SS Cyril and Methodius University,
Rudjer Bošković Street, 16,
Skopje 1000, R. N. Macedonia
e-mail: anita@tmf.ukim.edu.mk

Petre Makreski
Institute of Chemistry,
Faculty of Natural Sciences and Mathematics,
SS Cyril and Methodius University,
Arhimedova Street, 5,
Skopje 1000, R. N. Macedonia
e-mail: petremak@pmf.ukim.mk

Gennaro Gentile
Institute for Polymers, Composites and Biomaterials,
National Research Council of Italy,
Via Campi Flegrei 34, Comprensorio "A. Olivetti",
Pozzuoli, Napoli 80078, Italy
e-mails: gennaro.gentile@ipcb.cnr.it;
gennaro.gentile@cnr.it

Structural Changes of TiO_2 as a Result of Irradiation by E-Beam and X-Rays

The subject of this research was to monitor and evaluate the effect of X-rays and e-beam irradiation on the structure of nanoscaled TiO_2 and its properties. The samples of nanoscaled TiO_2 were synthesized using the sol–gel method and subsequently exposed to thermal treatment to obtain the anatase crystalline structure. X-ray powder diffraction (XRPD) and Raman spectroscopy revealed the following changes in the structure as a result of the e-beam and X-ray irradiation: a decrease in the size of the crystallite of TiO_2, an increase of the distance between the crystalline planes and the lattice parameters as well as the achievement of a certain degree of amorphization. As a consequence of the structural changes, thermal stability decreased. Also, a shift of the light absorption toward the visible end of the spectrum was detected and the energy of the band gap was reduced, indicating a better photocatalytic activity, i.e., the photocatalytic action can be shifted to the region of the visible light. [DOI: 10.1115/1.4046944]

Keywords: materials processing, metals, polymers, ceramics, intermetallics, and their composites

Introduction

Titania, the naturally occurring oxide of titanium, as inexpensive, innocuous, physically and chemically stable with a variety of structural forms and environmentally friendly material, has demonstrated a wide range of applications such as pigments, sunblocking material in cosmetics, optical devices, sensors, and medicine for artificial bones [1]. In recent decades, it attracts great attention in photocatalysis for the photocatalytic degradation of different degradable organic pollutants, photocatalytic water splitting, and solar energy conversion [2–6].

Among the three most known crystalline forms of TiO_2 (brookite, anatase, and rutile), anatase and rutile are mostly exploited for photocatalytic purposes. Anatase has been proven as a better photocatalyst than rutile despite its higher band gap energy (3.2 eV for anatase versus 3.0 eV for rutile) [7] justified by the following clarifications [7–9]: (i) as a result of the higher Fermi level compared to those of rutile, anatase shows higher adsorption affinity to the hydroxyl groups and lower affinity to oxygen adsorption; (ii) due to lower temperatures of production, anatase has smaller particles than those of rutile and consequently higher specific surface area and surface adsorption capacity; and (iii) anatase has an indirect band gap opposed to rutile's direct band gap. In the case of the indirect band gap, the excited electron can be stabilized at the lower level in the conduction band, which causes its longer life and higher mobility.

TiO_2 is considered a semiconductor with wide band, and therefore, activation might occur under ultraviolet (UV) light which limits its photocatalytic application under visible light, especially for solar conversion purposes. Several approaches are suggested to overcome these limitations such as (i) the addition (doping) of different anions (N, C, F, and B) or cations (Fe, Co, Ni, and Cr), causing lattice defects during the doping, mainly oxygen vacancies, which promote photocatalytic activity in the visible range of light [10]; (ii) using nonstoichiometric titanium oxides (Magneli phases) filled with lattice defects of oxygen vacancies type [11]; (iii) the treatment of TiO_2 by hydrogen plasma [12]; or (iv) irradiation of TiO_2 by ionizing radiation (electron beam, X-ray, or γ-ray) [13–15].

During irradiation, an interaction between applied rays and material arises at the atomic and crystalline lattice level, including the following effects [16]: (i) the displacement of atoms from the normal position, which can cause lattice vacancies, lodging interstitial locations, or interchange of dissimilar atoms in the crystalline lattice; (ii) ionization of atoms and formation of ion pairs; (iii) the production of impurities, that is, transformation of nuclei into other ones; and (iv) releasing high amount of energy at small volumes, which causes heating of the material. The most used ionizing radiations for materials treatment are categorized in two groups: corpuscular rays such as α-particles and β-particles (electrons or positrons) as well as electromagnetic waves such as X-rays and γ-rays [17,18]. The former are characterized by lower energy and penetration depth, while the latter demonstrate higher energy and penetration depth.

There are numerous works concerned with the improvement of photocatalytic characteristics of TiO_2 as a result of irradiation with e-beam [19–22], where the change of the Ti valence state (increasing of Ti^{3+}/Ti^{4+} ratio), the formation of oxygen vacancies, the decrease of band gap energy, and consequently, the increase of the photocatalytic activity were observed. The photocatalytic activity of titanium dioxide under X-ray irradiation holds promising opportunities for biomedical applications [23,24].

The subject of research in this study was observation of the structural changes and consequently changes of some properties (thermal and optical) of TiO_2 nanoparticles produced by own sol–gel

[1]Corresponding author.
Contributed by the Materials Division of ASME for publication in the Journal of Engineering Materials and Technology. Manuscript received March 13, 2020; final manuscript received April 5, 2020; published online April 18, 2020. Assoc. Editor: Pradeep Sharma.

procedure, as a result of the effects caused by X-ray and e-beam irradiation. Ionizing irradiation treatments were performed in order to establish whether they will be able to improve the photocatalytic characteristics of the nanostructured TiO_2.

Experimental

The investigated TiO_2 samples were prepared by the sol–gel procedure presented elsewhere [25]. Titanium tetraisopropoxide (TTIP) (Aldrich, 97%) was used as a precursor for the preparation of TiO_2. TTIP was dissolved in anhydrous ethanol (Merck, PA) in the ratio Ethanol:TTIP = 8:1. To provide the hydrolysis of TTIP, 1 M HNO_3 was added in a ratio of TTIP:HNO_3 = 10:1. This mixture was evaporated at 45 °C and ambient pressure with continuous stirring with 600–900 rpm until a fine nanoscaled, light yellow powder of $Ti(OH)_4$ was obtained.

According the thermal analysis [26], the $Ti(OH)_4$ powder was heated for 2 h in a chamber furnace in air atmosphere at 400 °C, as this is the temperature region of anatase stability.

The obtained TiO_2 powder was irradiated with a beam of 6 MeV electrons from a linear accelerator (ELU-6, Eksma, Russia). The dose rate was 100 Gy/s, as determined by calibrated polymer film dosimetry (B3000, B3WINdose Dosimeters), and the total absorbed dose was 50 and 500 kGy. A fraction of the TiO_2 powder was independently treated with X-ray irradiation with a dose of ~7 mGy. The tubes filled with nanoparticles were exposed to X-ray irradiation in the medical computed tomography scanner (in air atmosphere) separately. The tube voltage was set on 140 kV, and the tube current fixed at 200 mA.

The identification of the present structure phases and structural analysis was performed by X-ray powder diffraction (XRPD), Raman spectroscopy, and transmission electron microscopy (TEM).

X-ray powder diffraction measurements were carried out by a Rigaku Ultima IV diffractometer equipped with Cu$K\alpha$ radiation (λ = 1.54178 Å) obtained from an X-ray tube operating at 40 kV and a current of 30 mA. The $K\beta$ filter was used and the following optics were applied: divergence slit 2/3 deg, divergence height slit 10 mm, and scattering slit 8 mm. The diffraction data were collected over a 2θ range from 10 to 90 deg at a constant rate of 5 deg/min using a D/teX Ultra high-speed, position-sensitive linear (1D) detector. The average crystallite size was calculated from the broadening of the XRPD peaks using Scherrer's equation [27]. Furthermore, interplanar distance and lattice parameters were also calculated [28].

Non-polarized Raman spectra were recorded on micro-Raman multichannel spectrometer Horiba JobinYvonLabRam 300 Infinity. The Raman effect was excited by 632.8 nm laser line from a He:Ne laser without the use of a filter. For magnification, a ×50 objective was selected from an Olympus MPlanN confocal microscope. In order to focus the laser beam, a confocal hole of approximately 2 μm was used and the position on the sample surface was adjusted using a motorized x–y stage. The Raman shift was calibrated with the Raman peak of silica wafer positioned at 520.7 cm^{-1}. The acquisition time and the accumulation number were set at 4 s and 5 scans, respectively, for achieving better signal-to-noise ratio.

The bright-field TEM analysis of the prepared samples was performed on a FEI Tecnai G12 Spirit Twin (LaB6 source) at 120 kV acceleration voltage. TEM images were collected on a FEI Eagle 4 k charge-coupled device camera. Before the analysis, the samples were dispersed in water, diluted at about 2 mg/mL, and collected by immersing carbon coated TEM copper grids in the aqueous dispersions [29].

The thermal stability of the TiO_2 samples was studied by means of thermogravimetric analysis/differential thermal analysis (TGA/DTA) measurements on a Perkin Elmer PYRIS Diamond Thermogravimetric/Differential Thermal Analyzer. About 20 mg of the studied material were heated at a temperature interval of 25–1000 °C by a heating rate of 10 °C/min in an atmosphere of nitrogen. Optical properties were investigated by UV–Vis spectroscopy. The UV–Vis absorption spectra of TiO_2–water suspension were collected using a Varian Cary Scan 50 spectrophotometer (Switzerland) in 1 cm quartz cells, at 25 °C in the range of 200–900 nm with a scan speed of 200 nm.

Results and Discussions

X-ray powder diffraction spectra of the studied TiO_2 nanoparticles are shown in Fig. 1. For all studied samples, a total of 12 high or less pronounced peaks characteristic for the anatase crystalline form were detected. This means that the sol–gel procedure performed in oxygen atmosphere at 400 °C resulted in the fabrication of anatase as the sole product.

The non-irradiated sample showed more pronounced and intensive diffraction peaks than the irradiated ones. The decrease of intensity and the broadening of the peaks can be attributed to a decrease in crystallinity of the irradiated samples and to lowering the size of TiO_2 crystallites. The least pronounced peaks and the noise of the XRPD spectrum of the sample irradiated with X-ray point out to some degree of amorphization, especially evidenced in the increase of the baseline curvature in the 20–35 deg section. According to the literature [16,30], the disorder within the crystalline structure can be attributed mainly to atom displacement from the normal position, creating lattice vacancies or interstitial locations [16]. Under ionizing irradiation, some of the Ti^{4+} ions can be either reduced to Ti^{3+} or oxygen vacancies can be created [30]. Table 1 summarizes the values of crystallite size (D), interplanar distance ($d_{\{h,k,l\}}$), and lattice parameters (a and c, for the tetragonal system), calculated using the following equations:

$$D = \frac{K \cdot \lambda}{\mathrm{FWHM} \cdot \cos\theta} \tag{1}$$

$$2 \cdot d_{\{h,k,l\}} \cdot \sin\theta = n \cdot \lambda \tag{2}$$

$$\frac{1}{d_{\{h,k,l\}}} = \frac{h^2 + k^2}{a^2} + \frac{l^2}{c^2} \tag{3}$$

where K is the constant (0.94), λ is the X-ray wavelength (1.54178 Å), FWHM is full width at half maximum of the peak considered for calculation, θ is the angle of diffraction peak, n is the positive integer, $\{h,k,l\}$ are Miller indices of the corresponding crystal plane, and a and c are unit cell parameters of the tetragonal crystal system of anatase.

As it can be seen from Table 1, the size of the crystallites of the non-irradiated sample is ~17 nm. As a result of the action of

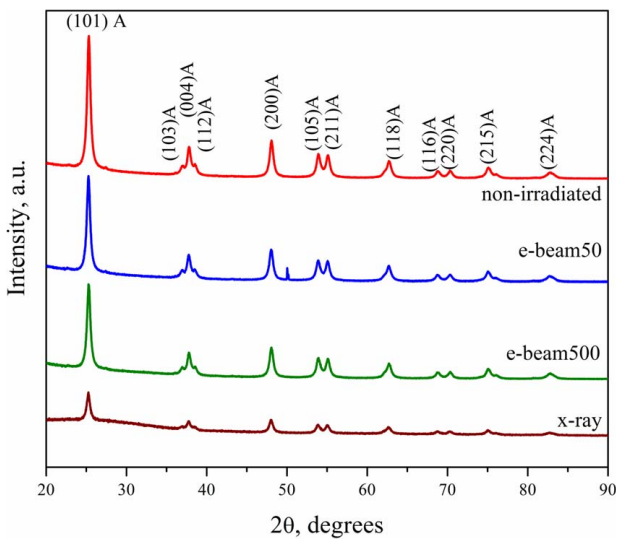

Fig. 1 XRPD patterns of the studied TiO_2 samples

Table 1 Changes of interplanar distance, lattice parameters, and crystallite size of the studied TiO_2 samples

Samples	2θ	$\{h,k,l\}$	FWHM	d-space (Å)	a (Å)	c (Å)	D (nm)	D (nm)
Non-irradiated	25.31	{101}	0.494	3.5175	3.7832	9.5546	17.22	16.87
	48.08	{200}	0.551	1.8916			16.52	
E-beam 50	25.27	{101}	0.540	3.5229	3.7860	9.6182	15.76	16.01
	48.04	{200}	0.559	1.8930			16.27	
E-beam 500	25.30	{101}	0.556	3.5187	3.7844	9.5547	15.31	15.12
	48.07	{200}	0.609	1.8922			14.94	
X-ray	25.26	{101}	0.602	3.5245	3.7874	9.6278	14.12	14.525
	48.02	{200}	0.6122	1.8937			14.85	

ionizing radiation, the size of the crystallites decreases. The greatest reduction of the crystallites, of more than 2 nm, associated to most relevant peak broadening in the XRPD spectrum, is recorded for samples treated by X-ray irradiation. The size reduction of the TiO_2 crystallites is less pronounced in the case of e-beam irradiation. Also, as a result of irradiations, interplanar distance and lattice parameters show an increase and are most pronounced for the X-ray irradiated sample. These changes in the crystalline lattice are most probably a result of the previously mentioned phenomena of the atom displacement and creation of lattice vacancies.

Figure 2 shows bright-field TEM images of the studied samples. Samples are constituted by agglomerate of TiO_2 primary particles with spherical shape, relatively uniform in size with some small deviation toward larger or smaller particles. The dimensions of the primary particles well fit the values of the crystallite sizes calculated by the Sherrer equation.

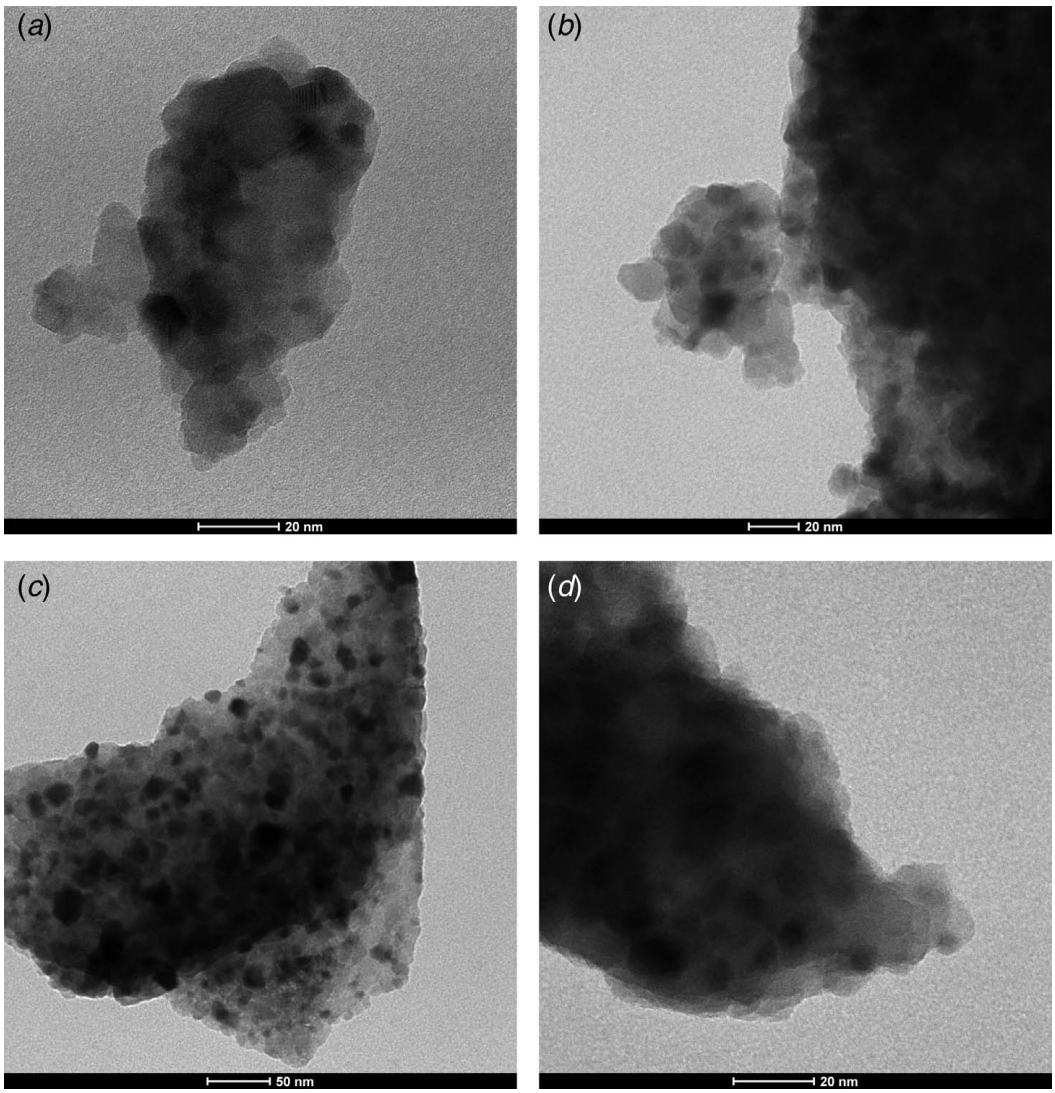

Fig. 2 Bright-field TEM images of the studied TiO_2 samples: (*a*) non-irradiated, (*b*) irradiated with e-beam (50 kGy), (*c*) irradiated with e-beam (500 kGy), and (*d*) irradiated with X-ray radiation (7 mGy)

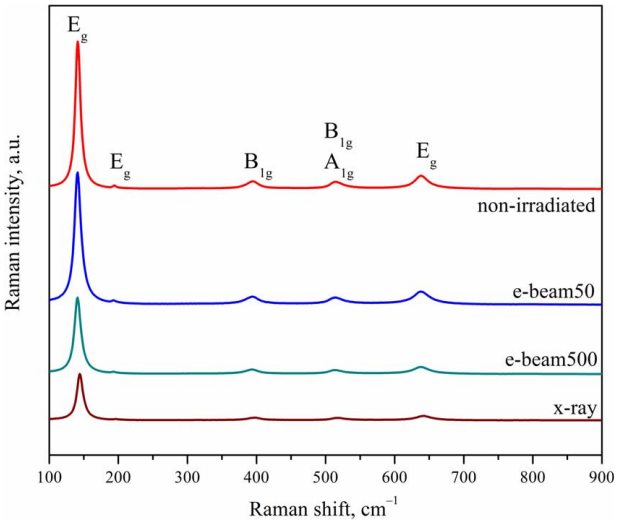

Fig. 3 Raman spectra of the studied TiO_2 samples

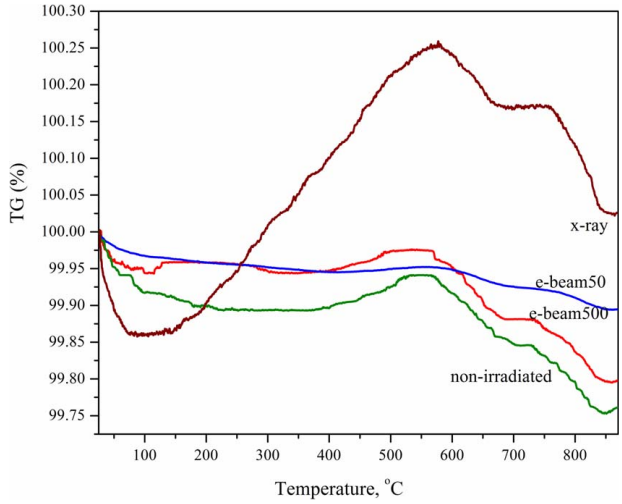

Fig. 4 TGA spectra of the studied TiO_2 samples

The exclusive existence of the anatase crystalline structure of the studied samples was also confirmed by Raman spectroscopy (Fig. 3). Namely, Raman spectra correspond to the well-known spectrum of anatase single crystal identified by Oshaka et al. [31] consisted of several Raman vibration modes: three E_g positioned at 144, 197, and 639 cm^{-1}, B_{1g} positioned at 399 cm^{-1}, and doublet of A_{1g} and B_{1g} at 514 cm^{-1} [31]. Congruent to the XRPD spectra, the non-irradiated sample shows most pronounced peaks (Raman vibration modes). Following irradiation of the sample, the spectra become less intensive and band broadening is observed, which is most prominent in the sample irradiated with X-rays. Also, it is evident that the positions of corresponding Raman vibration modes are shifted to higher wave numbers for irradiated samples compared to those of non-irradiated analog. According to the phonon confinement model, highly ordered structure exhibits phonon conservation, expressed with sharp and intensive peaks in the Raman spectrum. As disordering in the crystals (vacancies and interstitials) is evidenced, the crystallites size decreases in line with the increase of the phonon momentum distribution, which results in the broadening of the Raman peaks that shift to higher wave numbers [32–34]. Because the difference in the crystallites size between non-irradiated and irradiated samples is not so pronounced, the shift of the Raman vibration modes can be ascribed to the defects in the structure (oxygen vacancies and interstitials) caused by the irradiation. Table 2 unites the positions of the first, the most prominent E_g band for the studied samples. The highest shift is registered in the X-ray irradiated sample, which is in accordance with XRPD analysis.

Figure 4 depicts the TG curves for studied TiO_2 samples. The weight loss close to 100 °C corresponds to desorption of the physically adsorbed water in all studied samples as a result of the contact with nitrogen flow [35]. Near 150 °C, desorption of the surface-adsorbed water is complete and decomposition of the chemisorbed water (residual OH^-groups from $Ti(OH)_4$ and residual organic functional groups) took place [36]. The very low weight loss in this region indicates low quantity of these groups in the samples. From this temperature until ~500 °C, a small weight increase (0.05–0.10%) was observed for the non-irradiated and the e-beam irradiated samples. This increase can be ascribed to the gas sorption into the amorphous fraction of TiO_2 before the anatase/rutile transformation starts. This weight increase is most pronounced for the X-ray irradiated sample (about 0.4%), which points out that the structure of this sample is the most disordered and more prone to adsorb gas before the phase transformation occurs. Therefore, at higher temperatures, close to 650 °C, transformation of anatase to rutile can be observed [25,37], and at ~800 °C, TiO_2 is completely transformed to rutile.

Figure 5 systematizes UV–Vis spectra of the studied samples. By withdrawing tangents to the abscissa (inset in Fig. 5), the cutoff wavelengths (absorbance maxima) were determined [38]. The energy of band gap can be calculated using the following equation:

$$E_g = \frac{h \cdot c}{\lambda_0} \quad \text{(J)} \tag{4}$$

where h is the Planks constant (6.626×10^{-34} J s), c is the speed of light ($\sim 3 \times 10^8$ m/s), and λ_0 is the cutoff wavelength. Replacing the corresponding values for h and c, and considering the conversion

Table 2 Shift of the first Raman vibration mode (E_g, cm^{-1}) of the studied TiO_2 samples

Sample	E_g (cm^{-1})
Non-irradiated	140.99
E-beam 50	141.89
E-beam 500	141.89
X-ray	144.45

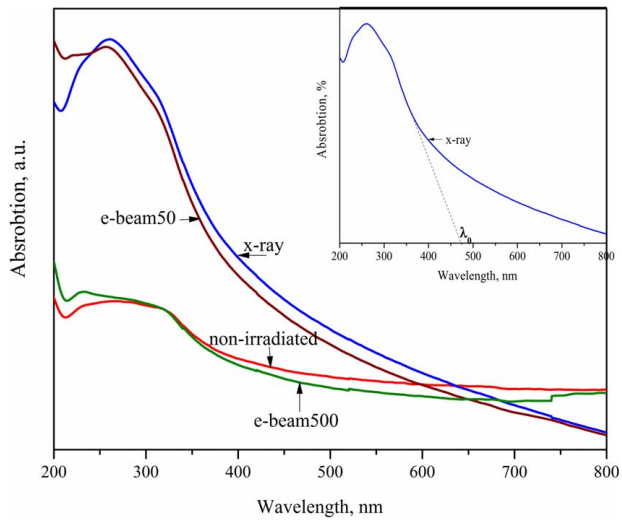

Fig. 5 UV–Vis spectra of the studied TiO_2 samples

Table 3 The values of the cutoff wavelength (λ_0, nm) and the calculated energy of the band gap (E_g, eV) for the studied samples

Sample	λ_0 (nm)	E_g (eV)
Non-irradiated	425	2.92
E-beam 50	453	2.74
E-beam 500	449	2.76
X-ray	482	2.57

factor for J to eV transformation, Eq. (4) obtains the form

$$E_g = \frac{1240.82}{\lambda} \quad \text{(eV)} \tag{5}$$

Corresponding values for the cutoff wavelength (λ_0) and the energy of band gap for each studied sample are shown in Table 3. These results pinpoint that the absorbance maxima (λ_0) of the irradiated samples was shifted to the higher wavelength (red-shift). As a consequence, the energy of band gap decreased (Eq. (5)), i.e., the photocatalytic activity of TiO_2 was shifted toward the region of the visible light. According to the literature [39], red-shifts can be ascribed mostly to oxygen vacancies in the crystal lattice acting as electron traps to yield Ti^{3+} and/or F-type color centers. This shift is most pronounced after X-ray irradiation, where the energy of band gap (E_g) decreases from 2.92 eV for the non-irradiated sample to 2.57 eV for the X-ray irradiated sample. The higher effect of X-ray in promotion of photocatalytic activity in the visible region, compared with that of e-beam irradiation, is due to the higher energy and greater penetrating ability of X-rays. Moreover, one can see that e-beam irradiation of 50 kGy has a similar effect of the e-beam of 500 kGy (E_g of 2.74 versus 2.76 eV, respectively). This points out that a dose of 50 kGy is sufficient to induce changes within the crystal structure of TiO_2 (the creation of oxygen vacancies and Ti^{3+} sites), whereas an additional dose of e-beam irradiation has no further influence on the structural changes.

Conclusions

The research presented in this paper, motivated by the idea to improve the photocatalytic activity of nanostructured TiO_2 produced by the sol–gel method using electron beam and X-ray irradiation, brought into light the following conclusions:

(1) XRPD analysis and Raman spectroscopy pointed out that electron beam and X-ray irradiation caused the reduction of the crystallites size and changes in the TiO_2 crystal lattice, probably such as the creation of oxygen vacancies and Ti^{3+} sites. These disorders in the structure were observed by the increase in interplanar distance, lattice parameters, and a shift of the Raman vibrational modes.
(2) These structural changes caused a red-shift increase of the absorbance maxima (λ_0) and consequently decreased the band gap energy. This is expected to promote TiO_2 photocatalytic activity in the visible light region.
(3) Much greater effect was achieved using X-ray irradiation as a result of its higher energy and greater penetration compared to the e-beam irradiation, although applied in lower dose (7 mGy of X-rays versus 50 or 500 kGy of e-beam).

Acknowledgment

This work has evolved from the Project "Application of Ionizing Irradiations in Nanotechnology for Environmental, Energy and Health purposes" (NANO IRRA NET), founded by the International Atomic Energy Agency (SV-MAK1003-1801824). The authors are very grateful to Professor Piotr Ulanski and Professor Sławomir Kadłubowski from Institute of Applied Radiation Chemistry, Faculty of Chemistry, Lodz University of Technology, Poland, for their help in e-beam irradiation of the samples. Also great thanks to Professor Violeta Vasilevska Nikodinoovska from SS Cyril and Methodius University, MedicalFaculty, Skopje, for her help in X-ray irradiation of the studied material.

References

[1] Diebold, U., 2003, "The Surface Science of Titanium Dioxide," Surf. Sci. Rep., **48**(5–8), pp. 53–229.
[2] Chen, X., and Mao, S. S., 2007, "Titanium Dioxide Nanomaterials: Synthesis, Properties, Modifications and Applications," Chem. Rev., **107**(7), pp. 2891–2959.
[3] Pelaez, M., Nolan, N. T., Pillai, S. C., Seery, M. K., Falaras, P., Kontos, A. G., Dunlop, P. S. M., Hamilton, J. W. J., Byrne, J. A., O'Shea, K., Entezari, M. H., and Dionysiou, D. D., 2012, "A Review on the Visible Light Active Titanium Dioxide Photocatalysts for Environmental Applications," Appl. Catal. B, **125**, pp. 331–349.
[4] Banerjee, A. N., 2011, "The Design, Fabrication, and Photocatalytic Utility of Nanostructured Semiconductors: Focus on TiO_2-Based Nanostructures," Nanotechnol. Sci. Appl., **4**(1), pp. 35–65.
[5] Dai, K., Peng, T., Ke, D., and Wei, B., 2009, "Photocatalytic Hydrogen Generation Using a Nanocomposite of Multi-Walled Carbon Nanotubes and TiO_2 Nanoparticles Under Visible Light Irradiation," Nanotechnology, **20**(12), p. 125603.
[6] Bak, T., Li, W., Nowotny, J., Atanacio, A. J., and Davis, J., 2015, "Photocatalytic Properties of TiO_2: Evidence of the Key Role of Surface Active Sites in Water Oxidation," J. Phys. Chem. A, **119**(36), pp. 9465–9473.
[7] Zhang, J., Zhou, P., Liu, J., and Yu, J., 2014, "New Understanding of the Difference of Photocatalytic Activity Among Anatase, Rutile and Brookite TiO_2," Phys. Chem. Chem. Phys., **16**(38), pp. 20382–20386.
[8] Banerjee, S., Gopal, J., Muraleedharan, P., Tyagi, A. K., and Raj, B., 2006, "Physics and Chemistry of Photocatalytic Titanium Dioxide: Visualization of Bactericidal Activity Using Atomic Force Microscopy," Curr. Sci., **90**(10), pp. 1378–1383.
[9] Luttrell, T., Halpegamage, S., Tao, J., Kramer, A., Sutter, E., and Batzill, M., 2014, "Why is Anatase a Better Photocatalyst Than Rutile?—Model Studies on Epitaxial TiO_2 Films," Sci. Rep., **4**, p. 4043.
[10] Zaleska, A., 2008, "Doped-TiO_2: A Review," Recent Pat. Eng., **2**(3), pp. 157–164.
[11] Toyoda, M., Yano, T., Tryba, B., Mozia, S., Tsumura, T., and Inagaki, M., 2009, "Preparation of Carbon-Coated Magneli Phases Ti_nO_{2n-1} and Their Photocatalytic Activity Under Visible Light," Appl. Catal. B, **88**(1–2), pp. 160–164.
[12] An, H., Park, S. Y., Kim, H., Lee, C. Y., Choi, S., Lee, S. C., Seo, S., Park, E. C., Oh, Y., Song, C., Won, J., Kim, Y. J., Lee, J., Lee, H. U., and Lee, Y., 2016, "Advanced Nanoporous TiO_2 Photocatalysts by Hydrogen Plasma for Efficient Solar-Light Photocatalytic Application," Sci. Rep., **6**, p. 29683.
[13] Kim, M. S., Jo, W. J., Lee, D., Baeck, S., Shin, J. H., and Lee, B. C., 2013, "Enhanced Photocatalytic Activity of TiO_2 Modified by e-Beam Irradiation," Bull. Korean Chem. Soc., **34**(5), pp. 1397–1400.
[14] Priyanka, K. P., Joseph, S., Sunny, A. T., and Varghese, T., 2013, "Effect of High Energy Electron Beam Irradiation on the Optical Properties of Nanocrystalline TiO_2," Nanosyst. Phys. Chem. Math., **4**(2), pp. 218–224.
[15] Diab, K. R., Doheim, M. M., Mahmoud, S. A., Shama, S. A., and El-Boohy, H. A., 2017, "Gamma-Irradiation Improves the Photocatalytic Activity of Fe/TiO_2 for Photocatalytic Degradation of 2-Chlorophenol," Chem. Mater. Res., **9**(9), pp. 49–60.
[16] Holbert K.E., 2008, "Radiation Effects and Damage. Dr. Holbert's Course "EEE 598—Radiation Effects", School of Electrical, Computer and Energy Engineering. Arizona State University," http://holbert.faculty.asu.edu/eee560/eee560.html
[17] Vasile C., and Butnaru E., 2017, "Radiation Chemistry of Organic Solids," *Applications of Ionizing Radiation in Materials Processing*, Vol. 1, Y. Sun, A. G. Chmielewski, eds., Institute of Nuclear Chemistry and Technology, Warsaw, pp. 117–141.
[18] Kashiwagi, M., and Hoshi, Y., 2012, "Electron Beam Processing System and Its Application," SEI Tech. Rev., **75**, pp. 47–54.
[19] Wronski, P., Surmacki, J., Abramczyk, H., Adamus, A., Nowosielska, M., Maniukiewicz, W., Kozanecki, M., and Szadkowska-Nicze, M., 2015, "Surface, Optical and Photocatalytic Properties of Silica-Supported TiO_2 Treated With Electron Beam," Radiat. Phys. Chem., **109**, pp. 40–47.
[20] Latthe, S. S., An, S., Jin, S., and Yoon, S. S., 2013, "High Energy Electron Beam Irradiated TiO_2 Photoanodes for Improved Water Splitting," J. Mater. Chem. A, **1**(43), pp. 13567–13575.
[21] Jun, J., Dhayal, M., Shin, J., Kim, J., and Getoff, N., 2006, "Surface Properties and Photoactivity of TiO_2 Treated With Electron Beam," Radiat. Phys. Chem., **75**(5), pp. 583–589.
[22] Hou, X., and Liu, A.-D., 2008, "Modification of Photocatalytic TiO_2 Thin Films by Electron Beam Irradiation," Radiat. Phys. Chem., **77**(3), pp. 345–351.
[23] Schmidt-Stein, F., Hahn, R., Gnichwitz, J., Song, Y. Y., Shrestha, N. K., Hirsch, A., and Schmuki, P., 2009, "X-Ray Induced Photocatalysis on TiO_2 and TiO_2 Nanotubes: Degradation of Organics and Drug Release," Electrochem. Commun., **11**(11), pp. 2077–2080.

[24] Molina Higgins, M. C., and Rojas, J. V., 2019, "X-Ray Radiation Enhancement of Gold-TiO_2 Nanocomposites," Appl. Surf. Sci., **480**, pp. 1147–1155.
[25] Paunović, P., Grozdanov, A., Češnovar, A., Ranguelov, B., Makreski, P., Gentile, G., and Fidančevska, E., 2015, "Characterization of Nano-Scaled TiO_2 Produced by Simplified Sol-Gel Method Using Organometallic Precursor," ASME J. Eng. Mater. Technol., **137**(2), p. 021003.
[26] Češnovar, A., Paunović, P., Grozdanov, A., Makreski, P., and Fidančevska, E., 2012, "Preparation of Nano-Crystalline TiO_2 by Sol-Gel Method Using Titanium Tetraisopropoxide (TTIP) as a Precursor," Adv. Nat. Sci.: Theory Appl., **1**(2), pp. 133–142.
[27] Cullity, B. D., 1978, *Elements of X-Ray Diffraction*, Addison-Wesley Publishing Company, Inc., London, UK.
[28] Castaldo, R., Lama, G. C., Aprea, P., Gentile, G., Ambrogi, V., Lavorgna, M., and Cerruti, P., 2019, "Humidity-Driven Mechanical and Electrical Response of Graphene/Cloisite Hybrid Films," Adv. Funct. Mater., **29**(14), p. 1807744.
[29] Castaldo, R., Lama, G. C., Aprea, P., Gentile, G., Lavorgna, M., Ambrogi, V., and Cerruti, P., 2018, "Effect of the Oxidation Degree on Self-Assembly, Adsorption and Barrier Properties of Nano-Graphene," Microporous Mesoporous Mater., **260**, pp. 102–115.
[30] Khan, M. M., Ansari, S. A., Pradhan, D., Ansari, M. O., Han, D. H., Lee, J., and Cho, M. H., 2014, "Band Gap Engineered TiO_2 Nanoparticles for Visible Light Induced Photoelectrochemical and Photocatalytic Studies," J. Mater. Chem. A, **2**(3), pp. 637–644.
[31] Oshaka, T., Izumi, F., and Fujiki, Y., 1979, "Raman Spectrum of Anatase TiO_2," J. Raman Spectrosc., **7**(6), pp. 321–324.
[32] Xu, C. Y., Zhang, P. X., and Yan, L., 2001, "Blue Shift of Raman Peak From Coated TiO_2 Nanoparticles," J. Raman Spectrosc., **32**(10), pp. 862–865.
[33] Choi, H. C., Jung, Y. M., and Kim, S. B., 2005, "Size Effects in the Raman Spectra of TiO_2 Nanoparticles," Vib. Spectrosc., **37**(1), pp. 33–38.
[34] Smith, K. A., Savva, A. I., Deng, C., Wharry, J. P., Hwang, S., Su, D., Wang, Y., Gong, J., Xu, T., Buttf, D. P., and Xiong, H., 2017, "Effects of Proton Irradiation on Structural and Electrochemical Charge Storage Properties of TiO_2 Nanotube Electrodes for Lithium-Ion Batteries," J. Mater. Chem. A, **5**(23), pp. 11815–11824.
[35] So, W. W., Park, S. B., Kim, K. J., Shin, C. H., and Moon, S. J., 2001, "The Crystalline Phase Stability of Titania Particles Prepared at Room Temperature by the Sol-Gel Method," J. Mater. Sci., **36**(17), pp. 4299–4305.
[36] Mehranpour, H., Askari, M., Sasani Ghamsari, M., and Farzalibeik, H., 2010, "Study on the Phase Transformation Kinetics of Sol-Gel Drived TiO_2 Nanoparticles," J. Nanomater., **2010**(6), p. 626978.
[37] Lee, M. S., Lee, G. D., Park, S. S., and Hong, S.-S., 2003, "Synthesis of TiO_2 Nanoparticles in Reverse Microemulsion and Their Photocatalytic Activity," J. Ind. Eng. Chem., **9**(1), pp. 89–95.
[38] Dharma J., Pisal A., 2012, UV/Vis/NIR Spectrometer, Application Note, PerkinElmer, Inc. Shelton, CT, https://www.perkinelmer.com/lab-solutions/resources/docs/APP_UVVISNIRMeasureBandGapEnergyValue.pdf
[39] Kuznetsov, V. N., and Serpone, N., 2009, "On the Origin of the Spectral Bands in the Visible Absorption Spectra of Visible-Light-Active TiO_2 Specimens Analysis and Assignments," J. Phys. Chem. C, **113**(34), pp. 15110–15123.